ASME-ATI-UIT 2015 Conference on Thermal Energy Systems: Production, Storage, Utilization and the Environment
17 – 20 May, 2015, Napoli, Italy

ENERGY SAVINGS AND INCREASED ELECTRIC VEHICLE RANGE THROUGH IMPROVED BATTERY THERMAL MANAGEMENT

Joshua Smith*, Michael Hinterberger*, Christoph Schneider*, Juergen Koehler °

* AUDI AG, 85045 Ingolstadt (Germany)
° University of Braunschweig, Hans-Sommer-Str. 5, 38106 Braunschweig (Germany)

ABSTRACT

Lithium-Ion cells are temperature sensitive: operation outside the optimal operating range causes premature aging and correspondingly reduces vehicle range and battery system lifetime. In order to meet consumer demands for electric and hybrid-electric vehicle performance, especially in adverse climates, a battery thermal management system (BTMS) is often required.

This work presents the analysis of various cooling plate concepts using an a novel cell model. For each concept, the input parameters (ambient temperature, coolant temperature and coolant flow rate) are varied and the resulting effect on the average temperature and temperature distribution across and between cells is compared. Additionally, the pressure loss along the coolant path is utilized to determine energy efficiency. Using this methodology, various cooling plate layouts optimized for production alternative techniques are compared to the state of the art. It is shown that these production-optimized cooling plates provide sufficient thermal performance with the additional benefit of mechanical integration within the battery and/or vehicle system. It is also shown that the coolant flow influences battery cell thermal behavior more than the solid material, and that pressure drop is more sensitive to geometrical changes in the cooling plate than temperature changes at the module.

Keywords: *Lithium-Ion; Thermal management; Electric vehicle.*

1. INTRODUCTION

The temperature sensitivity of Lithium-Ion cells, exemplified through capacity degradation and safety risks, has been thoroughly demonstrated in the literature [2, 7, 14, 26]. Cold weather and consumer requirements such as rapid charging often mandate a BTMS, but economic BTMS production is often challenging. Development costs are high, and thermal simulation models require experimental validation for maximum accuracy. Testing an unrefined BTMS with high-power Lithium-Ion cells can be dangerous, especially in the case of a system failure resulting in a short circuit between cells. In order to reduce the size, weight, energy consumption, and cost of the total battery system, new thermal management concepts must be identified and analyzed.

The presented experimental method is based on the simulation of the thermal behavior of a cell with a so-called "Smart Battery Cell" (SBC). The SBC has been designed to eliminate the disadvantages associated with experiments using actual battery cells. As a result, BTMS produced using alternative techniques can be quickly compared in an early state of development in order to guide further design iterations.

1.1 Methods for the Experimental Analysis of a BTMS

A complete experimental comparison of battery thermal management systems requires both a detailed analysis of the effect on the battery and of the thermal management concept performance.

In order to measure the effect on the battery, the temperature resulting at the cell as a result of the thermal management system must be determined. In order to compare various systems, it is desirable to repeatedly measure the temperature at the same location and under the same boundary conditions. Comparing thermal management systems via simulation models eliminates the cost and infrastructure of an experimental setup; however, the accuracy of a simulation depends on the accuracy of the inputs. For example, a large source of error is the thermal contact interface, which is difficult to calculate. The effect of the thermal contact interface can however be isolated and observed in experimental trials. For this reason, a hardware-based thermal model of the cell is chosen.

Most analyses of cell characteristics or behavior found in the literature use actual cells. Arguably the simplest and most prevalent method for measuring the effect of a thermal management system on battery cells is by attaching thermocouples at various positions over the cell casing. Countless experiments are performed in this way, as thermocouples of varying size and accuracy are commercially available. However, some thermal management concepts include small gaps between cells and various components, making the integration of thermocouples at all desired locations difficult. The required electrical insulation between the thermocouple and the cell can affect thermal contact surfaces, resulting in altered behavior. The placement of a thermocouple in the exact same position on a cell in diverse thermal management concepts may not be possible due to interference with other components. Essentially, thermocouples themselves are not the problem, but rather their use on the exterior of the cell. Additional experimental methods considered for the comparison of the effect of thermal management systems on battery cells are briefly discussed below.

Thermal imaging is a useful non-invasive technique that has been effectively implemented for single cells and groups of cells [9, 20, 22]; however, the surface analyzed must be visible to the camera, meaning that temperatures and gradients for example directly between two cells or between cells and BTMS cannot be measured.

Calorimetry has been used to determine the heat loss of a cell (or cells) very precisely under defined loads, and to then approximate the heat transfer coefficient and cell temperature using a lumped capacitance method [1, 20]. This method is useful for determining for example total energy removal, but

cannot isolate local gradients and discrepancies between- and across individual cells that lead to premature aging.

Recently, much research has been conducted in the field of electrochemical impedance spectroscopy measurements for determining the internal temperature of actual cell [21–23]. While temperature differences between cells can be measured, gradients over the individual cells such a local hotspots induced by a thermal management system cannot be determined.

In-situ temperature measurements using thermocouples or temperature sensors within the cell provide data at the critical chemically active layers, allowing local temperatures to be measured. This technique has been applied on numerous cell types [10, 15, 18, 29, 30]; however, using actual cells carries the increased cost of additional experimental trials due to the variance in cell behavior and cannot be implemented with new, unrefined thermal management concepts safely (e.g. because of coolant leakage). Additionally, the presence of thermocouples or similar within the active chemical layers can influence cell behavior.

1.2 Disadvantages of Using Actual Battery Cells

In addition to the difficulty in measuring temperatures and temperature gradients over and between actual battery cells, further characteristics of large format Lithium-Ion cells make experimental trials difficult, dangerous, and time consuming. For example, compromising the electrical insulation or inducing high temperatures in any way can result in severe safety risks: not only is the electrical energy in large format cells high, but far more the chemical energy released during failure proposes a significant safety hazard. As previously mentioned, the temperature sensitivity of the Lithium-Ion cells results in varying thermal behavior depending on the travel, use, and storage history of the cell. To compare only the effect of thermal management concepts, many additional trials are required to eliminate the statistical variance caused by each cell's individual history. Testing the robustness of a BTMS by simulating a damaged or prematurely aged cell is also difficult to perform reproducibly. By avoiding the use of actual cells, experimental safety and reproducibility can be realized far more quickly and efficiently in an earlier stage of BTMS development.

Alternatives to actual cells are presented in the literature primarily for the analysis of the performance a specific thermal management concept [3, 16, 17, 25, 27]. In these cases, only two to three cells are considered. This small-scale does not accurately capture the effect of a thermal management concept on a module, or more precisely the susceptibility to inhomogeneous aging.

Accurate and validated hardware-based cell models are rare in comparison. Wang et. al. (2014) use a casing filled with Atonal 324 to simulate the thermal capacity of the actual cell analyzed [27]. Lukhanin et. al. (2012, 2013) utilize a heating plate and various layers to simulate the thermal properties of a pouch cell; however, the temperature sensors are included on the surface, which disturbs the thermal contact interface [3, 16, 17]. No examples of temperature sensors integrated into the hardware-based model are known to the author. The potential for integrated sensors is a significant advantage of a hardware-based model over an actual cell.

Based on the state-of-the-art of battery and thermal management systems analyses, a novel hardware-based cell model is presented.

2 NOVEL METHOD FOR COMPARING THERMAL MANAGEMENT SYSTEMS

In order to efficiently isolate the effect of various thermal management systems on actual cells, the use of a "Smart Battery Cell" (SBC) is proposed. The goal of the SBC is to:

- Replicate the thermal behavior of the actual cell;
- Provide reproducible conditions and thereby eliminate the variances in thermal behavior of actual cells;
- Ensure safety during testing: for example allowing new BTMS concepts to be tested in a prototype phase;
- Provide enhanced data acquisition and measurement capacity for comparing the effect of thermal management concepts "one-to-one."
- Allow for a large amount of trials in rapid succession without sacrificing reproducibility or accuracy
- Simulate a damaged or aged cell and determine the effect on other cells and the reaction of the BTMS

The steps required to develop the aforementioned SBC, and to ensure equivalent thermal behavior to an actual cell, are highlighted in the following sections

2.1 Determining the Thermal Behavior of an Actual Cell

The first step for the development of the SBC is the analysis of the actual cell type that is to be replicated. A prismatic high capacity PHEV cell is the focus of this research, but this method can be applied to other cell formats and chemistries.

The goal of the experimental analysis is to investigate cell thermal behavior at the casing, under the premise that an automotive OEM will source and not produce battery cells. Because the size of the PHEV-2 cell considered, both the average temperature and the temperature distribution must be considered. Pesaran et. al. have measured the effects of current collector tab orientation on temperature distribution in a cell, indicating the significance of the geometry especially in large-format cells [20]. Robinson et. al. have used x-ray micro tomography to visualize the geometry and noted localized heat generation at certain components [22]. Additionally, because of the dynamic nature of a battery system in operation, a stationary model is insufficient. The experimental procedure is designed under the assumption is that if the SBC can dynamically match the thermal behavior of the actual cell in various test conditions, it will act similarly to the actual cell when combined to a module or when integrated with a BTMS.

2.2 Experimental Analysis of the Thermal Behavior

The experimental setup utilizes 40 Type-K Ni-Cr Ni thermocouples to measure the temperature (and distribution thereof) over the cell. 24 thermocouples are fitted onto the large "front" face of the cell, four on both "sides", five on the "bottom", one near each terminal, as shown in Fig. 1.

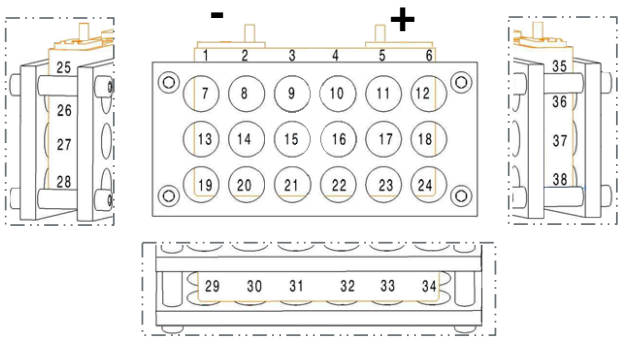

Fig. 1: Position of the thermocouples over the surface of the cell (numbered one through 38, plus one near each terminal). The modified compressive bracing required for safety is also shown [24].

Unfortunately, the cell requires a bracing for safety during operation and storage because of the generated forces, and the resulting damage that can occur to the cell's active layers. The required safety bracing has however been redesigned to accommodate as many thermocouples as possible and facilitate the use of thermal imaging.

Between the bracing and the cell is a 5mm polycarbonate plate to thermally and electrically insulate the bracing from the cell. This insulation serves to mitigate the influence of the bracing on the cell; this is verified via thermal imaging. The temperature is logged over a CAN-Bus to a PC that is time-synchronized with the high-voltage (HV) testing equipment.

The HV-power source is connected to the cell terminals via over-dimensioned cables, as a small cable diameter would disturb the temperature profile of the cell due to the joule heating in the cable. The entire setup is placed in the middle of a CTS 200 Liter climate chamber with temperature and humidity control. Because the climate chamber regulates temperature via a fan, an inconsistent airflow and therefore changing coefficient of heat transfer could influence the average temperature and the temperature distribution, and inhibit the comparison between trials. Therefore, the tests are performed in wind-still conditions at constant relative humidity (40%). To facilitate the wind still condition reproducibly, the chamber and experimental setup are climatized over night to ensure that the entire cell, and not just the casing, are at the same temperature. At the start of the test, when the battery cell cycling begins, the active climitazation is turned off and remains so for the duration of the test.

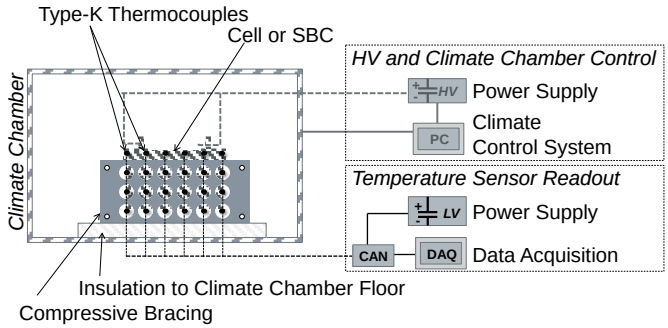

Fig. 2: Experimental set-up used for the analysis of actual cell behavior and validation of SBC behavior. The high-voltage connections are replaced with the SBC-connections for the validation of the SBC.

Additionally, the large volume of the climate chamber in comparison to the cell size means air temperature differences over the test time are minimal. The same natural convection boundary condition is implemented for the module-level comparisons, but due to the size of the experimental setup, a specially designed climate chamber is used (Section 3.3).

Each experiment begins with a fully charged cell (100% SOC, 4.1 V). The cell is the discharged to 20% SOC, and recharged to 100% SOC repeatedly for a total duration of four hours. This process is repeated at various rates C-rates (1, 2, 3, 4, 5 and 6 C), where "C" indicates the capacity of the cell. Thus, for the considered 25 Ah cell, a charging rate of 1 C is equal to 25 A, while a rate of 2 C is equal to 50 A. As a result, more cycles are achieved in the four hour test time at higher charge/discharge rates. After four hours of cycling, the cells are left in the wind-still climate chamber in order to observe the cool-down behavior.

Five new cells were tested three times at each charge/discharge rate to reduce the effect of variances in cell thermal behavior, which is influenced by the travel, use, and storage history of the cell [14]. The temperature gradients are measured throughout the test via the thermocouples (on five of the sides) and thermal imaging. Contour plots of the measured temperature and the thermal images are used to analyze the temperature distribution, while the measured temperature alone is used to determine the average cell temperature. This analysis was performed within the scope of a master's thesis [24].

2.3 Design of the Smart Battery Cell

The SBC consists of an Aluminum core having approximately the same shape as the actual cell's jelly roll except with thin channels, allowing for the simple integration of thermocouples and heating elements (Fig. 3). The core also contains insulating coatings and air gaps to replicate the thermal mass, heat capacity, and thermal conductivity of the actual cell. Integrated cooling channels allow for rapid reconditioning between tests, significantly increasing the amount of experimental trials that can be performed per day. Distributed over the Aluminum core within individual channels are 16 thermocouples (eight per side). The heating element, a thin adhesive pad consisting of eight zones, sits over the thermocouples on the core. The heating zones are used to produce heat equivalent to the heat loss of an actual cell. Actual cell data is drawn from the a multitude of individual cell tests, thereby eliminating the variance caused by performing an experiment with various actual cells. As a result, far less trials are required to isolate the influence of the BTMS.

The core, including the connections for the internal cooling channels, the wiring for the heating element, and the measurement equipment, is connected to the cell lid. The cell lid, containing a flange, slides within the original cell casing and electrical insulation. Care is taken to insulate the data acquisition equipment from the power source in order to avoid electromagnetic interference in the measurements.

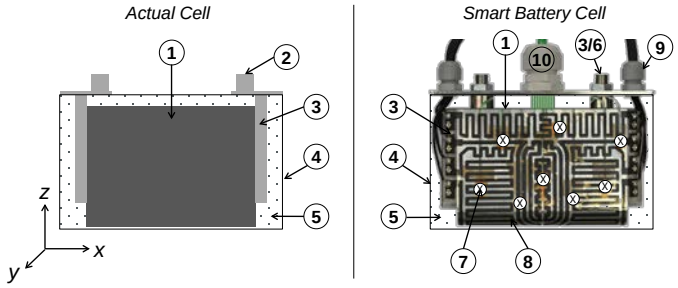

Fig. 3: Schematic view of the actual cell (left) showing the jelly-roll (1), terminals (2), current collector tabs (3), casing (4), and air gaps (5). The SBC (right) shown with the additional features of an internal cooling circuit (6) with connections mimicking the current collector tabs, 16-integrated temperature sensors (eight per side) marked with an "X" (7), 8-heating zones per cell (8) including the required wiring (9), and the connection for the thermocouple wiring (10).

Multiple design iterations were undertaken to realize these functionalities [24]. The respective SBC iteration was then tested against the actual cell using the same experimental setup as for the classification of the actual cell. The performance of the final version of the SBC is shown in Fig. 4.

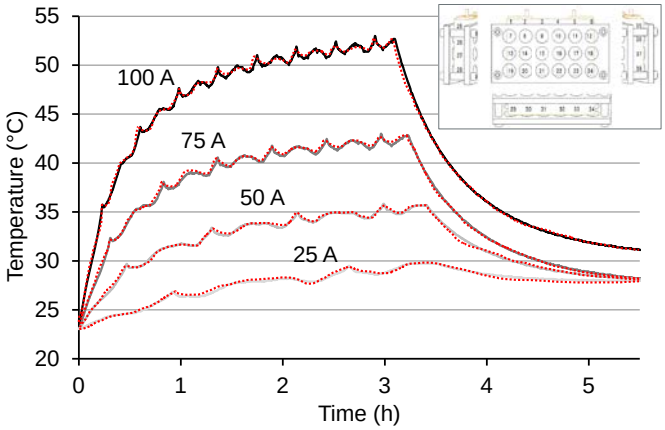

Fig. 4: Comparison of the average temperature over the surface of an actual cell (solid-line) and the SBC (dashed-line) under identical experimental conditions and charging/discharging rates [24].

Using the internal geometry of the cell as a reference, and accurate hardware-based model of a PHEV-2 cell is realizable. The dynamic thermal performance, especially in the cool-down phase, indicates similar thermal characteristics to the actual cell. Using the integrated thermocouples of the SBC, the effect of various thermal management concepts on the cell can be quantified experimentally. By means of the internal coolant circuit of the SBC, reproducible initial conditions are quickly reached, allowing for far more trials to be performed.

Many manufacturers utilize so-called battery modules as building blocks for a complete battery system. These building blocks can then be combined in various configurations to realize an array of battery systems for different vehicle. Because the module is the building block of many battery system variations, the module-level is the most universal level at which to compare thermal management concepts. In this research, the eight-SBCs are combined to a module.

3 EXPERIMENTAL ANALYSIS OF COOLING PLATE THERMAL BEHAVIOR

Though many diverse cooling plate layouts are possible, some common features and design guidelines exist. A cooling plate utilizes a coolant to transfer heat to and from the battery. Currently, a water-glycol mixture or a refrigerant (such as R134a or 1234yf) are commonly used in production vehicles. In either case, the leak-tightness of the cooling plate (and complete circuit) is critical to protect against coolant leaking on the battery and potentially causing a short circuit. Because absolute leak-tightness does not exist, an acceptable value and correspondingly an appropriate test method must be selected [13]. Leak-tightness is influenced by cooling plate layout and production technique selection to ensure that, for example, the joining of two pieces meets the leakage specification. Forces within the cooling plate are a function of the pressure created by the coolant in the cooling plate channels, which is again a function of the channel size and the required inlet pressure to overcome the pressure drop from pump outlet to inlet. Selection of the appropriate production technique and the corresponding cooling plate design to meet the specified leak-tightness is critical.

A cooling plate must also thermally contact the cells. Better thermal contact translates directly to more efficient BTMS performance [8]. This contact interface is however complicated by the required electrical insulation between cells, and by the manufacturing tolerances of the battery cell casings and of the cooling plate. Thus, the acceptable deformation during the production process and the resulting flatness tolerance for the final product must be established. As with any production process, tighter tolerances generally correlate to additional production steps and higher production costs. The tolerance compensation and electrical insulation of the cells occur at the same interface: between cooling plate and cell. This additional layer(s) create an additional contact resistance, as shown in Equation 3.7:

$$R = \frac{t_{layer}}{k_{layer} A_{contact\ surface}} \quad (1)$$

where t_{layer} is the layer thickness, k_{layer} the thermal conductivity and $A_{contact\ surface}$ the area of the contact surface. Thus, assuming the contact area is given, either the thermal conductivity of the material must be raised and/or the thickness of the layer must be decreased. In all cases, air gaps, which have a very low conductivity (0.02 $W^1m^1K^1$ under standard conditions and pressure) should be avoided, as they can create local hot-spots and temperature gradients across the module. Very thin (0.01 to 0.1 mm) electrically insulating foils or coatings from the consumer electronics industry generally have low thermal conductivity (0.1 to 0.2 $W^1m^1K^1$), but are not ductile and therefore cannot compensate for short-wave tolerances. Thicker thermal pads have conductivities over an order of magnitude higher (3 to 5 $W^1m^1K^1$), and are available in various thicknesses to compensate tolerances; however, the force required to compress the pad does not scale linearly with surface area. Therefore, the module and cooling plate must be designed to handle the resulting forces. Thermal pastes with similar conductivities to the pads are also prevalent due to the lower costs versus a pad and the lower forces required to compress an initially liquid material. The electrical resistance is however not guaranteed by the paste because of the dispersion or uneven spreading during application. Thus a means of securing against a short circuit, such as an electrically

insulating film, must be used in conjunction. Thermal pastes also pose a challenge in the production and most likely require automation to achieve adequate process stability. In all cases, a reduction of the layer thickness and reduction in the air gaps can additionally be achieved through enhanced contact pressure between the cells and the cooling plate [5, 11, 28]; however, as mentioned, the module and cooling plate must then be designed for the resulting mechanical load.

3.1 Analysis Criteria

This research is based on a production-oriented analysis with the primary goal of reducing system costs by minimizing production complexity. Additional components not critical to cell function and safety should be minimized. For this reason, the basis for the thermal analysis of thermal management systems is a module with no thermal management.

Not only the average temperature, but also the temperature differences between individual cells are relevant to total system performance. Cells are electrically contacted in series to raise the system voltage, and in parallel to raise the system capacity. When connected in series, the "chain" formed is susceptible to the failure of a single cell. Aging of a single cell additionally lowers the total system voltage, and thereby the vehicle range [12]. Additionally, when chains of cells connected in series are connected together in parallel, each cell voltage must be monitored to ensure an equivalent voltage [12]. As a result, all undamaged cells must be balanced to the same voltage, which can result in a significant reduction of vehicle range. In this research, the quantity Δ(ΔT) quantifies the effect of a thermal management system in facilitating premature aging. The term compares the temperature gradients over each individual cell (ΔT) to one another, thereby expressing the susceptibility of the cells in the module to age at different rates. Because the temperature is measured experimentally, the normal or Gaussian distribution is most commonly applicable [6]. Calculating the standard deviation instead of purely the difference between the maximum and minimum temperature serves to eliminate data outliers from the 128 measurement points throughout the module. Furthermore, the SBC contains 16 measurement points on the cell jelly-roll: because this is a small percentage of the total volume, the sample standard deviation Eq. (2) is used, which corrects for the fact that the true jelly roll mean temperature is not known [19].

$$s_{cell} = \sqrt{\frac{1}{\mathrm{n}-1}\left(\sum_{t=1}^{n}(X_t - \bar{X})^2\right)} \tag{2}$$

Using the sample standard deviation (s) instead of the sample standard variance (s^2) ensures that the units of the comparison are in Kelvin as measured experimentally [19]. Furthermore, to account for the temperature difference over the majority of the jelly roll excluding outliers, three times the standard deviation is used, which includes 99.7% of the jelly roll. To compute $\Delta(\Delta T)$, the difference between maximum and minimum individual cell variance is taken.

$$\Delta(\Delta T) = 3(s_{Cell})_{max} - 3(s_{Cell})_{min} \tag{3}$$

Plots of $\Delta(\Delta T)$ as a function of time are shown to exhibit the effect of various thermal management systems on temperature homogeneity and premature aging.

The theoretical hydraulic work (P) is calculated as an indication of the energy consumption of a thermal management system.:

$$P = \dot{V}\,\Delta p \tag{4}$$

and is a function of the volumetric flow rate of the coolant ($\dot{V}$) and the pressure drop over the circuit (Δp). A lower theoretical hydraulic work indicates an energy savings. Eq. (4) thereby considers both the contribution of the BTMS flow channel layout/geometry (Δp) and the required operating conditions ($\dot{V}$) to the energy consumption.

3.2 Experimental Setup

The SBC is utilized in a specially designed climate chamber that guarantees still air at constant temperature. The experimental setup is designed to isolate the effect of the BTMS on the SBC.

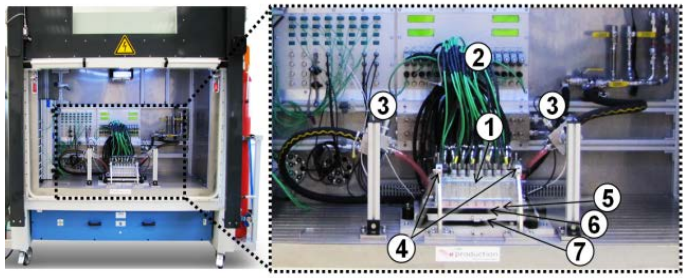

Figure 5: Left, the climate chamber, and right a close-up view of the experimental setup for testing a cooling plate, showing (1) 8-SBC module, (2) connections to SBC, (3) water-glycol circuit temperature and pressure measurement points, (4) bracing for applying contact pressure (onto cooling plate), (5) cooling plate, (6) thermal contact pad, and a (7) stiff, thermally insulated backing for cooling plate.

The reference module is placed on a POM base in the center of the test stand. The SBCs are connected (thermocouples, power source and hydraulic lines) in their corresponding positions. The climate chamber temperature is then set and using the hydraulic circuit in the SBC, the test module and the climate chamber are brought to the desired test temperature. When the measured temperature of each thermocouple is within 1°C, the trial is manually started.

In addition to the climate chamber temperature, a heat loss profile for the SBCs is required as an experimental input. The heat loss profile of the SBC replicates the heat loss of an actual cell. The heat loss of the cell is calculated using a one-dimensional cell model as a function of the instantaneous current, voltage, and state of charge of the test vehicle's battery system. The temperature is held constant at ambient in the model used. For the experimental trials, the single cell heat loss profile is split identically over the individual heat zones of the SBC, and each SBC is run at the same heat loss profile. The heat loss profile used (Fig. 6) is a function of the ambient temperature of the test.

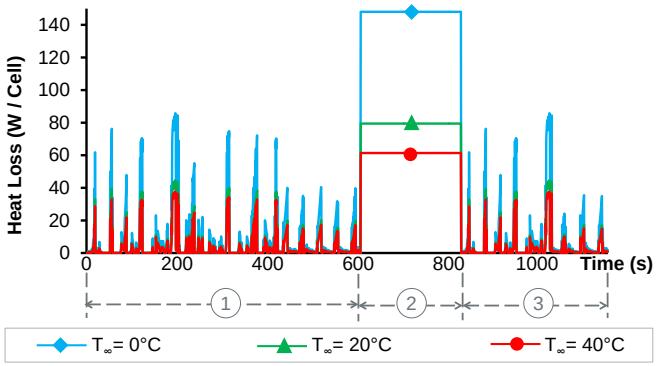

Fig. 6: Heat loss profile used in the experimental trials at the three ambient temperatures considered. Three drive cycle segments designed to explore various characteristics are: aggressive city and country driving section (1), rapid charging rate / aggressive racetrack performance (2), and an additional aggressive city and country drive (3).

The heat loss profile stems mostly from actual vehicle trials, and is designed to explore the dynamic behavior of the thermal management system. This drive cycle provides a demanding yet still feasible for a high-performance PHEV.

The trials are repeated at climate chamber temperatures of 0°C, 20°C and 40°C. Relative humidity is measured but not varied. The next trial is started when all thermocouples are within 1°C of one another. Three trials were performed at each temperature, with trials at a given climate chamber temperature performed sequentially (i.e. three times at 20°C, then three times at 40°C) in order to increase experimental efficiency by not reconditioning the entire chamber. The hydraulic circuit of the SBC also serves to cut reconditioning times significantly. Coolant flow speed and inlet temperature are varied as well.

3.3 Cooling Plate Designs Considered

Three cooling plate designs based on various production techniques were conducted in cooperation with partners in the research project *eProduction*. The criterion of a total thickness of 5 mm or smaller was established to facilitate better vehicle integration. Friction Stir Welding (FSW) and variations thereof, Electron Beam Welding (EBW), and Adhesion were analyzed for their suitability for low-thickness cooling plates. The process of soldering itself was not analyzed within the scope of this project, but sample cooling plates were tested experimentally for thermal performance and energy consumption. So-called technology demonstrators are created to test the designs. The production techniques are not discussed in detail in this work, but rather the resulting layouts.

Cooling plate technology demonstrator 1. The first cooling plate technology demonstrator uses fluid displacing bodies (FDB) with the goal of providing the mechanical structure to resist internal pressure spikes, and to enhance the heat transfer between the coolant and cells. The fluid channel volume is high in relation to the solid material. The position of the inlet and outlet, shown in Fig. 7, create a flow pattern known as an "I-flow."

Cooling plate technology demonstrator 2. The second technology demonstrator has a narrow channel of constant width that meanders multiple times under the cells (as opposed to cooling plate technology demonstrator 3). This design leaves more solid material to stiffen the cooling plate. The inlet and outlets are attached on the same side (so-called U-flow) of the cooling plate, as shown in Fig. 7, resulting in a so-called "U-flow" pattern.

Cooling plate technology demonstrator 3. The final design was chosen to represent the state of the art in cooling plate manufacturing. The flow channel is a simple U created from extruded aluminum channels. The extruded aluminum profiles only partially cover the base of the module, as shown in Fig. 7. The "partial" contact to the battery module has been chosen to determine if the weight savings are realized at the cost of thermal performance. A U-flow inlet/outlet position is used.

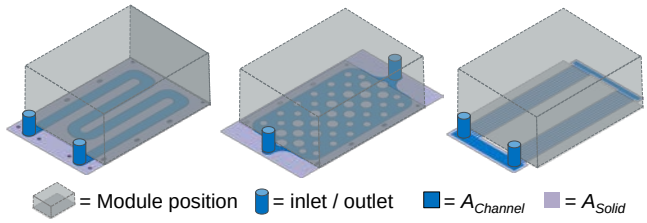

Fig. 7: The three cooling plate technology demonstrators (1-3, left to right) analyzed experimentally. The position of the module on the cooling plate is shaded.

For the experimental trials, a Berquist Gap Pad 5000 S35 provides the thermal contact and electrical insulation between the module and cooling plate. The compression force is held constant at all four corners of the module for each trial, and the cooling plate is stiffened with an insulated backing in order to eliminate the deflection as a variable.

3.4 Experimental Results

In order to visually compare the performance of each technology demonstrator across various ambient temperatures, the module average temperature and temperature differences ($\Delta(\Delta T)$) are plotted for a constant inlet temperature and flow rate.

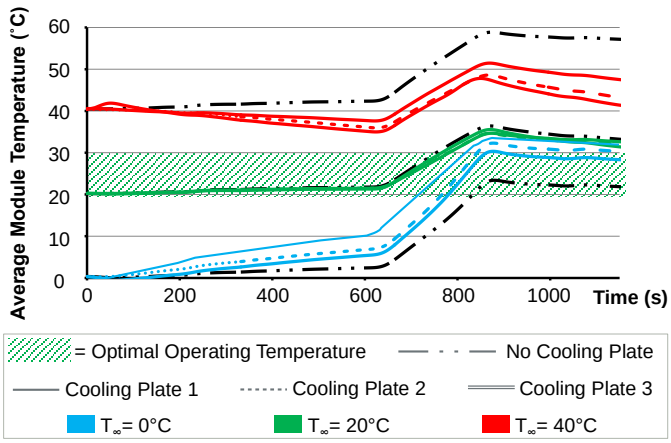

Fig. 8: Average module temperature for a constant coolant flow rate (5 L^1min^{-1}) and inlet temperature (20°C). The average temperature for a module without thermal management is shown in as a reference. The driving cycle phases (1-3) are labeled.

Cooling plate technology demonstrator 1 is most effective at transferring heat between the module and the coolant to maintain the optimal cell operating temperature. However, the enhanced heat transfer through the bottom of the module comes at a price: the temperature differences between cells increase significantly.

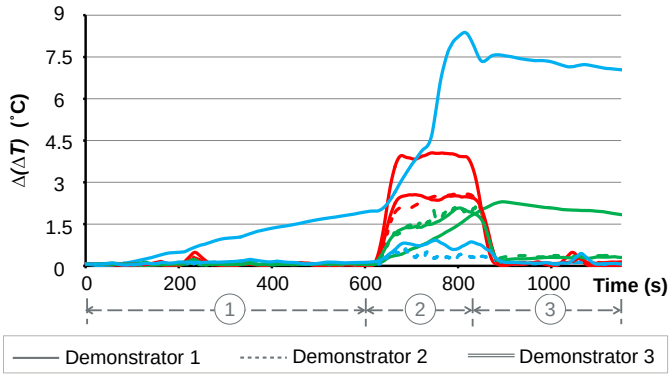

Fig. 9: Temperature differences between cells at the same boundary conditions as in Fig. 8. The driving cycle phases (1-3) are labeled.

The temperature differences and the average temperature are most sensitive to coolant temperature changes in cooling plate technology demonstrator 1. To determine the source of this sensitivity, the design must be abstracted. Because all technology demonstrators consist of a 1 mm aluminum top-plate and a 1 mm gap pad between coolant and module, the thermal conductivity (k_{layer}) and thickness (t_{layer}) are equivalent. However, the footprint of the coolant channel ($A_{contact\ surface}$, as viewed in Fig. 7)—and therefore the total thermal conductivity—is different between designs (Eq. 1).

The energy consumption is compared via the theoretical hydraulic work (Eq. 4). This comparison for all inlet and ambient temperatures at flow rates near 5 L/min is shown in Fig. 10.

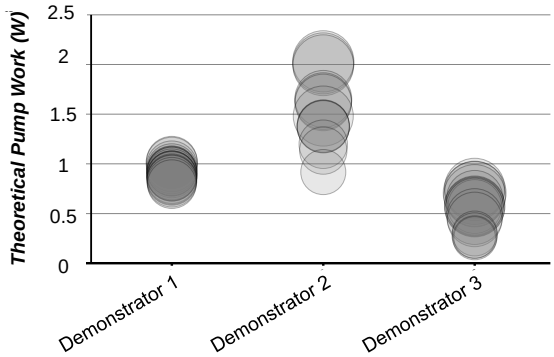

Fig. 10: Theoretical pump work for the cooling plate technology demonstrators analyzed. The circle size indicates the volumetric flow rate.

Across all conditions tested, cooling plate 2 has the highest energy consumption as a result of the long channel length (high pressure drop). The FDB in cooling plate 1 create higher pressure losses than the smooth channels of cooling plate 3, even with the shorter channel length resulting from the I-flow pattern.

The thermal performance of cooling plates 2 and 3—as measured by the module average temperature and $\Delta(\Delta T)$—are very similar, while the energy consumption is much higher in cooling plate 2, highlighting the high sensitivity of pressure drop versus thermal performance to channel geometry. Thus, the simple U-flow layout is preferable to a serpentine-like channel, especially when the channel footprint is increased in respect to the amount of solid material. The use of FDB and an I-flow, as shown in cooling plate 1, can greatly enhance heat transfer, but the result is a higher $\Delta(\Delta T)$, which facilitates inhomogeneous cell aging.

4 CONCLUSION

The best compromise between average temperature, temperature differences between cells, and energy consumption is a simple U-flow. Pressure drop is far more sensitive to geometrical variations than the thermal behavior of the cells. Maximizing the channel height within the constrictions of the total cooling plate height further reduces pressure loss. The U-flow layout allows for the inlet and outlet to be positioned on the same side, resulting in additional volume on only one side of the cooling plate, facilitating better vehicle integration. Cooling plates produced with alternative production technique (cooling plate 1 and 2) can meet and exceed the thermal behavior of the state of the art cooling plate, with the additional benefit of structural integration within the vehicle or battery system. However, the optimization of the pressure drop by reducing the channel length is necessary in order to not compromise vehicle range. In all cases, cooling plate design must occur in conjunction with the layout of the thermal interface between cells and cooling plate. This layer must minimize thermal resistance in order to increase the efficiency of the cooling plate.

ACKNOWLEDGMENTS

This research was funded by the German Federal Ministry of Education and Research (BMBF) within the scope of the project *eProduction*.

The authors wish to acknowledge the investigation of the production techniques performed by research project partners, including: Andreas Roth (TU München), Marc Essers (RWTH Aachen), Andreas Track (FEES Verzahnungstechnik GmbH), Uwe Maurieschat and Christian Schuch (Fraunhofer IFAM).

NOMENCLATURE

Symbol	Quantity	SI Unit
A	Surface area	m^2
k	Thermal conduction	$W^1\ m^{-1}\ K^{-1}$
t	Thickness	m
R	Thermal Resistance	$K^1\ W^{-1}$
s_{cell}	Sample standard deviation	K
$\Delta(\Delta T)$	Temperature difference b/w cells	K
P	Power	W
$\dot{V}$	Flow rate	$L^1\ min^{-1}$
Δp	Pressure drop	mbar
η	efficiency	none
Bi	Biot Number	none
L	Length	m
h	Coefficient of Convection	$W^2\ m^{-1}\ K^{-1}$

REFERENCES

[1] S. Al Hallaj, J. Prakash, and J. Selman, "Characterization of commercial Li-ion batteries using electrochemical–calorimetric measurements," *Journal of Power Sources*, vol. 87, no. 1-2, pp. 186–194. DOI: 10.1016/S0378-7753(99)00472-3.

[2] T. M. Bandhauer, S. Garimella, and T. F. Fuller, "A Critical Review of Thermal Issues in Lithium-Ion Batteries," *J. Electrochem. Soc*, vol. 158, no. 3, pp. R1-R25. DOI: 10.1149/1.3515880.

[3] A. Belyaev and D. Fedorchenko et al, Investigation of Heat Pipe Cooling of LI_ION Batteries. Available: https://www.bnl.gov/isd/documents/86095.pdf (2015, Feb. 22).

[4] P. Childs, "Advances in temperature measurement," vol. 36, pp. 111–181. DOI: 10.1016/S0065-2717(02)80006-5

[5] N. Daubitzer, M. Engelhart, T. Heckenberger, and T. Himmer, Device for Pressing a cooler against a Battery. Patent WO2012/104394A1. Issued August 9, 2012.

[6] K. Eden and H. Gebhard, Eds, *Dokumentation in der Mess- und Prüftechnik: Messen - Auswerten - Darstellen Protokolle - Berichte - Präsentationen*. Wiesbaden: Vieweg+Teubner Verlag / Springer Fachmedien Wiesbaden GmbH, Wiesbaden, 2012.

[7] M. Fleckenstein, O. Bohlen, and B. Bäker, "Aging Effect of Temperature Gradients in Li-ion Cells Experimental and Simulative Investigations and the Consequences on Thermal Battery Management,"The 26th International Battery, Hybrid and Fuel Cell Electric Vehicle Symposium. Los Angeles, California, USA, May. 6, 2012.

[8] L. S. Fletcher, "Recent Developments in Contact Conductance Heat Transfer," *J. Heat Transfer*, vol. 110, no. 4b, p. 1059. DOI: 10.1115/1.3250610.

[9] M. R. Giuliano, A. K. Prasad, and S. G. Advani, "Experimental study of an air-cooled thermal management system for high capacity lithium–titanate batteries," *Journal of Power Sources*, vol. 216, pp. 345–352. DOI: 10.1016/j.jpowsour.2012.05.074.

[10] C. Heubner, M. Schneider, C. Lämmel, U. Langklotz, and A. Michaelis, "In-operando temperature measurement across the interfaces of a lithium-ion battery cell," *Electrochimica Acta*, vol. 113, pp. 730–734. DOI: 10.1016/j.electacta.2013.08.091

[11] S. Hirsch, C. Schmid, A. Wiebelt, and M. Stripf, Thermisch Übergangsvorrichtung, Temperierplatte und Energiespeichereinheit. German Patent DE102011084002A1. Issued April 4, 2013.

[12] U. Köhler, "Aufbau von Lithium-Ionen-Batteriesystemen," in *Handbuch Lithium-Ionen-Batterien*, R. Korthauer, Ed, Berlin, Heidelberg: Springer Berlin Heidelberg, 2013, pp. 95–106.

[13] P. Kritzer and O. Nahrwold, "Dichtungs- und Elastomerkomponenten für Lithium-Batteriesysteme," in *Handbuch Lithium-Ionen-Batterien*, R. Korthauer, Ed, Berlin, Heidelberg: Springer Berlin Heidelberg, 2013, pp. 119–129.

[14] B. Y. Liaw, E. P. Roth, R. G. Jungst, G. Nagasubramanian, H. L. Case, and D. H. Doughty, "Correlation of Arrhenius behaviors in power and capacity fades with cell impedance and heat generation in cylindrical lithium-ion cells," *Journal of Power Sources*, vol. 119-121, pp. 874–886. DOI: 10.1016/S0378-7753(03)00196-4.

[15] Z. Li, J. Zhang, B. Wu, J. Huang, Z. Nie, Y. Sun, F. An, and N. Wu, "Examining temporal and spatial variations of internal temperature in large-format laminated battery with embedded thermocouples," *Journal of Power Sources*, vol. 241, pp. 536–553. DOI: 10.1016/j.jpowsour.2013.04.117.

[16] A. Lukhanin, A. Belyaev, D. Fedorchenko, M. Khazhmuradov, O. Lukhanin, Y. Rudychev, and U. S. Rohatgi, "Thermal Characteristics of Air Flow Cooling in the Lithium Ion Batteries Experimental Chamber," in *Proceedings of the ASME summer heat transfer conference 2012: HT 2012, presented at ASME 2012 summer heat transfer conference, July 8-12, 2012, Rio Grande, Puerto Rico*, pp. 129–133.

[17] A. Lukhanin, A. Byelyayev, D. Fedorchenko, M. Khazhmuradov, O. Lukhanin, S. Martynov, Y. Rudychev, E. Sporov, and U. S. Rohatgi, "Investigation of Air Flow Cooling of Li-Ion Batteries," in *Proceedings of the ASME International Mechanical Engineering Congress and Exposition--2013*, New York, N.Y: American Society of Mechanical Engineers, 2014.

[18] M. S. K. Mutyala, J. Zhao, J. Li, H. Pan, C. Yuan, and X. Li, "In situ temperature measurement in Lithium Ion Battery by transferable flexible thin film thermocouples // In-situ temperature measurement in lithium ion battery by transferable flexible thin film thermocouples," *Journal of Power Sources*, vol. 260, pp. 43–49. DOI: 10.1016/j.jpowsour.2014.03.004.

[19] W. C. Navidi, *Statistics for engineers and scientists*. Boston, Mass: McGraw-Hill, ©2006.

[20] A. Pesaran, M. Keyser, K. Smith, G.-H. Kim, and S. Santhanagopalan, "Tools for Designing Thermal Management of Batteries in Electric Drive Vehicles,"Large Lithium Ion Battery Technology & Application Symposia Advanced Automotive Battery Conference. Pasadena, CA, USA, Feb. 4, 2013.

[21] L. Raijmakers, D. Danilov, J. van Lammeren, M. Lammers, and P. Notten, "Sensorless battery temperature measurements based on electrochemical impedance spectroscopy," *Journal of Power Sources*, vol. 247, pp. 539–544. DOI: 10.1016/j.jpowsour.2013.09.005.

[22] J. B. Robinson, J. A. Darr, D. S. Eastwood, G. Hinds, P. D. Lee, P. R. Shearing, O. O. Taiwo, and D. J. Brett, "Non-uniform temperature distribution in Li-ion batteries during discharge – A combined thermal imaging, X-ray micro-tomography and electrochemical impedance approach," *Journal of Power Sources*, vol. 252, pp. 51–57. DOI: 10.1016/j.jpowsour.2013.11.059.

[23] J. P. Schmidt, S. Arnold, A. Loges, D. Werner, T. Wetzel, and E. Ivers-Tiffée, "Measurement of the internal cell temperature via impedance: Evaluation and application of a new method," *Journal of Power Sources*, vol. 243, pp. 110–117. DOI: 10.1016/j.jpowsour.2013.06.013.

[24] C. Schneider. (2013). Analysen und Untersuchungen von Kühl- und Dichtsystemen bei Hochvolt-Batteriesystemen unter Berücksichtigung der Produktionsanforderungen für eine Serienfertigung. Unpublished master's thesis, Wilhelm Büchner Hochschule (Fachbereich Mechatronik), Darmstadt, Germany.

[25] T.-H. Tran, S. Harmand, B. Desmet, and S. Filangi, "Experimental investigation on the feasibility of heat pipe cooling for HEV/EV lithium-ion battery," *Applied Thermal Engineering*, vol. 63, no. 2, pp. 551–558. DOI: 10.1016/j.applthermaleng.2013.11.048.

[26] J. Vetter, P. Novák, M. Wagner, C. Veit, K.-C. Möller, J. Besenhard, M. Winter, M. Wohlfahrt-Mehrens, C. Vogler, and A. Hammouche, "Ageing mechanisms in lithium-ion batteries," *Journal of Power Sources*, vol. 147, no. 1-2, pp. 269–281. DOI: 10.1016/j.jpowsour.2005.01.006.

[27] Q. Wang, B. Jiang, Q. Xue, H. Sun, B. Li, H. Zou, and Y. Yan, "Experimental investigation on EV battery cooling and heating by heat pipes," Applied Thermal Engineering. DOI: 10.1016/j.applthermaleng.2014.09.083

[28] S. Weileder, S. Köster, R. Löffler, R. Lustig, and A. Meijering, Device for Supplying Power, Having a Cooling Assembly. Patent WO2012013315A1. Issued February 2, 2012.

[29] G. Yang, C. Leitão, Y. Li, J. Pinto, and X. Jiang, "Real-time temperature measurement with fiber Bragg sensors in lithium batteries for safety usage," *Measurement*, vol. 46, no. 9, pp. 3166–3172. DOI: 10.1016/j.measurement.2013.05.027.

[30] J. Zhao, H. Li, H. Choi, W. Cai, J. A. Abell, and X. Li, "Insertable thin film thermocouples for in situ transient temperature monitoring in ultrasonic metal welding of battery tabs," *Journal of Manufacturing Processes*, vol. 15, no. 1, pp. 136–140. DOI: 10.1016/j.jmapro.2012.10.002.